

The 2007 Caldera Collapse of Piton de la Fournaise Volcano: Source Process from Very-Long-Period Seismic Signals

Zacharie Duputel^{a,*}, Luis Rivera^a

^a*Institut de Physique du Globe de Strasbourg, UMR7516, Université de
Strasbourg/EOST, CNRS, Strasbourg, France.*

Abstract

In April 2007, Piton de la Fournaise volcano experienced its largest caldera collapse in at least 300 years. This event consisted of a series of 48 subsidence increments characterized by very-long-period (VLP) seismic signals equivalent to M_w 4.4 to 5.4. Source analysis of VLP events suggests a piston-like mechanism with a collapsing crack source corresponding to the contraction of the magma reservoir and a single force representing the collapse of the above rock column. We show that the collapse dynamics is primarily controlled by magma withdrawal from the reservoir, which was likely in a bubbly state at the time of the event. Similar to the 2018 Kilauea collapse, we observe a reduction of the time-interval between successive subsidence increments, which results from the acceleration of magma withdrawal and a progressive weakening of the edifice at the beginning of the sequence.

Keywords: Caldera collapse; Magma reservoir processes; Piton de la Fournaise; Single force source; Surface waves

*Corresponding author

Email address: zacharie.duputel@unistra.fr (Zacharie Duputel)

1. Introduction

Although caldera collapses are frequent in the evolution of basaltic systems, they have been monitored at only a few volcanoes worldwide (Filson et al., 1973; Kumagai et al., 2001; Michon et al., 2007; Sigmundsson et al., 2015; Neal et al., 2019). Such collapses usually consist of a quasi-periodic series of discrete subsidence events manifested by tilt steps and very long period (VLP) signals (e.g., Fontaine et al., 2014; Kumagai et al., 2001). While the initiation mechanisms of such phenomena remains largely enigmatic, they generally involve a lateral magma withdrawal from a subsurface reservoir through low elevation vents. Observations indicate a complex feedback process between summit collapses and the dynamics of the eruptive vent. While magma outflow from a sub-surface reservoir is usually associated with summit deflations (e.g., Epp et al., 1983), collapses can also act as a mechanism to push the magma out of the chamber. Effusive surges and short-term edifice inflations following summit collapses suggest a piston-like mechanism, in which the depressurized magma chamber is regularly repressurized by the subsiding rock column (Kumagai et al., 2001; Michon et al., 2011; Neal et al., 2019).

Caldera collapses involve different source processes like dip-slip motion on ring faults and the contraction of a magma reservoirs. These mechanisms are often modeled using moment tensor parameters, whose inversion on volcanoes usually yields vertical compensated-linear-vector-dipoles (CLVD) representing ring faulting (e.g., Shuler et al., 2013) or tensile crack sources associated with the pressurisation of magma reservoirs (Kumagai et al., 2001; Mildon et al., 2016). Such a moment tensor representation, however, ignores the

effects of the detached mass that can be significant during gravity-driven caldera collapses. As far as the excitation of long period seismic waves is concerned, the descending collapse rock column induces unloading and loading of the volcanic edifice that can be modeled with a single force (e.g., Takei and Kumazawa, 1994). Because volcanoes involve mass advection processes generating forces on the Earth, the modeling of volcanic sources commonly requires the consideration of single forces in addition to moment tensor components (Nakano et al., 2003; Chouet and Matoza, 2013). A remarkable example is the 1980 Mount St. Helens eruption (USA), which combined a massive landslide represented by a horizontal single force (Kanamori and Given, 1982) and a series of volcanic explosions corresponding to the superposition of an isotropic source and a vertical force (Kanamori et al., 1984). Other examples of volcanic phenomena inducing single forces are dome collapses (e.g., Uhira et al., 1994) or magma movements in the edifice (e.g., Chouet et al., 2010).

In this study, we focus on the April 2007 collapse that affected the summit area of Piton de la Fournaise volcano located on La Réunion island (France). Although numerous collapses have occurred in the summit area since the 18th century, the 2007 event is the largest collapse reported at Piton de la Fournaise (Michon et al., 2013). It followed a particularly active period with 4 eruptions in 10 months (Peltier et al., 2009) that ended in a lateral low-altitude eruption with exceptionally high flow rate and a large volume of ejected lava (Staudacher et al., 2009). Early geodetic co-eruptive measurements show a significant deflation of the volcano before the collapse (Peltier et al., 2009; Fontaine et al., 2014; Froger et al., 2015), suggesting that

the low-altitude eruption induced a sudden depressurization of the magma reservoir that ultimately resulted in the collapse of the rock column below the summit (Michon et al., 2007). This major failure within the edifice was accompanied by a sudden decrease of seismic velocities in the summit area (Duputel et al., 2009) and an exponentially decaying post-eruptive deflation of the central cone (Froger et al., 2015).

The surface collapse activity started on April 5 at 20:48 UTC with an earthquake of magnitude $M \sim 5$ that could be observed at teleseismic distances (Fig. 2 and Supplementary Fig. S1). This event was followed by more than 40 smaller collapses that occurred quasi-periodically until mid April 2007 (Michon et al., 2011; Fontaine et al., 2014). Each collapse was characterized by inflationary tilt steps and VLP signals (cf., supplementary Fig. S2; Fontaine et al., 2014). It was also accompanied by an intense microseismic activity below the volcano summit (Massin et al., 2011). The collapse resulted into a depression of ~ 330 m of the Dolomieu summit crater with a total volume similar to the bulk volume of emitted lava ($\sim 10^8$ m³; Michon et al., 2007; Urai et al., 2007; Staudacher et al., 2009). Although numerous studies have focused on geodetic deformation, seismicity and velocity variations associated with this activity (Peltier et al., 2009; Froger et al., 2015; Brenguier et al., 2008; Massin et al., 2011; Got et al., 2013), only a limited number of studies focused on the actual source mechanism of the VLP signals generated by collapse events (Fontaine et al., 2014, 2016). In this study, we thus combine near-field observations at the Geoscope station RER (8.5 km from the volcano summit) and surface waves observed at 25 teleseismic stations to investigate the source of collapse events that affected

Piton de la Fournaise in April 2017. To mitigate any bias due to the effect of lateral heterogeneities on teleseismic surface waves, our analysis accounts for 3D heterogeneities using the spectral element approach. We then explore different source representations to constrain the different source processes involved during the April 2007 caldera collapse.

2. Seismological observations and waveform simulations

We select 25 teleseismic broadband stations for which the VLP signal generated by the first collapse event is clearly visible. The resulting dataset has an azimuthal gap of 30° and is composed of stations within 90° of epicentral distances. Seismic waveforms are deconvolved to velocity and band-pass filtered between 50s and 100s. Periods shorter than 50s are filtered out to mitigate the effect of short-scale structural heterogeneities that are not resolved in global 3D velocity models. The 100s corner period reduces the effect of long-period noise, in particular for stations in Indian ocean southern islands and Antarctica (removing those stations would result in an azimuthal gap exceeding 130°). In the 50-100s period range, the observed seismograms are dominated by fundamental mode surface waves for which a significant fraction of the energy stays near the free surface where lateral structural heterogeneities are significant at global scale (e.g., due to oceans and continents). To account for such strong lateral variations, we conduct 3-D spectral-element simulations to compute the Green's functions used for source characterization (Komatitsch and Tromp, 1999). We assume a global 3-D Earth model composed of S40RTS (Ritsema et al., 2011) and Crust2.0 (Bassin et al., 2000).

We complement teleseismic records with near-field observations at the Geoscope station RER, located 8.5 km away from the Piton de la Fournaise summit area. Given its proximity to the source, the RER station provides direct information on the overall duration and centroid time of the source. It is modeled using Herrmann (2013) implementation of the wavenumber integration method for the local velocity model used at the Piton de la Fournaise Volcano Observatory (OVPF; model derived from Battaglia et al., 2005). We only use the vertical component seismogram and do not incorporate horizontal channels that are significantly contaminated by tilt signals (Fontaine et al., 2014). Before inversion, the seismogram is deconvolved to velocity and band-pass filtered in the period range of 5-100 s. The resulting waveform consists of a long-period signal with a relatively simple sinusoid pulse with a duration of ~ 17 s (see Supplementary Fig. S2).

3. Source mechanism of the first collapse event on April 5, 2007

As mentioned above, the April 2007 collapse can possibly involve different source processes that can be modeled at long period by a moment tensor source (e.g., slip on a ring fault, contraction of a magma reservoir) or by a single force (e.g., unloading and loading of the volcanic edifice by the detaching rock column). In the following, we confront these different source representations to the seismological observations of the first VLP event on April 5 at 20:48 UTC.

3.1. Moment tensor inversion

We employ a strategy similar to Duputel et al. (2016) where centroid moment tensor (CMT) parameters are inverted using surface waves in a 3-D

Earth model. The parameters to be determined are the 6 elements of the seismic moment tensor as well as the centroid location and source duration. Although we have tested different centroid locations, our tests show a very limited sensitivity of long period seismic waves to the source location at the 100 m scale of the Piton de la Fournaise summit area. We therefore fix the centroid below the Dolomieu summit crater (21.244°S , 55.714°E) and only grid-search for the best point-source depth (from 0.5 km to 3.5 km). The centroid time and duration are also estimated using a simple grid-search strategy assuming an isosceles triangular moment rate function (MRF). Our preferred CMT solution for the main April 2007 collapse is presented in Fig. 2a and Fig. 3a. The optimum centroid time is 20:48:49 UTC and the source half-duration is 3 sec (cf., Supplementary Fig. S3). We find a best point-source depth 2 km below the free surface (i.e. ~ 500 m above sea level). This estimate is however subject to large uncertainties as waveform fits are very similar if we change the source depth.

Although estimated posterior uncertainties are relatively small, results suggest a large negative correlation between isotropic and vertical compensated linear vector dipole (CLVD) components (cf., Supplementary Table S1). To explore the contribution of the isotropic component to fit the data, we conduct an inversion assuming the trace of the moment tensor to be zero (i.e., the deviatoric moment tensor). Results in the Supplementary Fig. S4 show that such source cannot fit the data properly, therefore confirming that an isotropic component is necessary to explain available observations. To further assess what mechanism is requested by our observations, we estimate the minimum RMS misfit associated with every type of moment tensor source

(cf., Supplementary Text S1). The resulting source-type diagram in Fig. 3b allows us to estimate what type of moment tensor source is consistent with the observed waveforms (Ford et al., 2010). Results suggest that the first collapse is consistent with a vertical closing crack, in agreement with the values and orientation of the principal axes in Fig. 3a. The source-type diagram in Fig. 3b also reveals uncertainty on the double-couple component of the source, which results from poor constraints on $M_{r\theta}$ and $M_{r\phi}$, due to the small amplitudes of the associated excitation kernels (see Table S1; Kanamori and Given, 1981).

3.2. *Single force inversion*

To investigate possible effects due to the unloading and loading of the collapsing rock column, we also perform a centroid single force (CSF) inversion using an approach similar to Kawakatsu (1989). At long period, the effect of a detached mass can be modeled by a single time-varying force (e.g., Kanamori and Given, 1982; Ekström and Stark, 2013). To represent the effect of the descending mass acceleration and deceleration, we assume a sinusoidal source time history such that the final integral of the force equal to zero (e.g., Kawakatsu, 1989). We invert for the 3 components of the peak force vector along with the source timing and duration.

Results in Fig. 4 indicates a predominantly vertical force vector that is consistent with the downward motion of the rock column (i.e., the initial upward orientation of the force is in the opposite direction of the accelerating rock mass). In agreement with the moment tensor inversion, we obtain a centroid time at 20:48:49 UTC and a half-duration of 4sec (cf., Supplementary Fig. S3b). As far as the overall fit is concerned, the CSF solution

in Fig. 2b seems to fit the data as well as the moment tensor model shown in Fig. 2a. The posterior correlation matrix presented in Supplementary Table S2 do not show significant correlations between the different components of the inverted peak force vector. If we constrain the force vector to be purely vertical, we do not notice a significant deterioration of the waveform fit (cf., Supplementary Fig. S5), which indicates that the small south-west component of the force in Fig. 4a is not required to fit the data. This is consistent with the fact that horizontal force components are associated with larger uncertainties (cf., Table S2).

3.3. Joint inversion of Moment tensor and force

We also conduct a joint inversion of moment tensor and force parameters. Given our limited sensitivity to the centroid depth and the force horizontal components, we assume a vertical force and fix the source 2 km below the free surface. We thus invert for the 6 elements of the moment tensor, the maximum force amplitude along with their centroid times and durations. The solution presented in Fig. 2c and Fig. 5 is obtained for a half-duration of 3 s for both single force and moment tensor sources (consistently with CMT and CSF solutions presented above).

The inverted focal mechanism in Fig. 5a is consistent with a vertically closing crack and is very similar to the one obtained in Fig. 3. The force source in Fig. 5b is consistent with a downward moving rock column as the single force model in Fig. 4. Optimum centroid times indicate that the closing crack source occurs ~ 2 s before the upward force is applied. The retrieved peak force amplitude is correlated with the moment tensor parameters (e.g., with the vertical CLVD component; cf., Supplementary Table S3). As in

Table S1, we also notice a large negative correlation between isotropic and vertical CLVD components. Despite these tradeoffs, Fig. 2 shows that this joint model yields to a better waveform fit at the near-field station RER compared to moment tensor and single force sources presented before.

4. Smaller collapse events from April 5 to 14, 2007

Although smaller collapses that followed the April 5 event are not visible at teleseismic distances, the associated VLP events are well recorded at the RER Geoscope station (e.g., Fontaine et al., 2014). To obtain a catalog of these smaller VLP events, we use the ObsPy implementation of the STA/LTA algorithm on the vertical component of RER between April 5 and April 14, 2007. We use a short time average (STA) window of 20s and a long time average of 400s with thresholds of 3.4 and 3.0 for on and off trigger times. This detection procedure results into a catalog of 48 collapse events (including the first collapse) that are listed in Supplementary Table S4.

As for the first collapse event, the subsequent smaller collapses manifest as relatively simple long-period waveforms. Supplementary Fig. S2 shows that waveforms generated by the successive collapses have a similar shape, indicating that these VLP events correspond to similar source mechanisms. We therefore fix the source geometry according to CMT and CSF models obtained for the first event and investigate smaller collapses by only inverting the source depth, timing, duration and size (i.e., seismic moment or force magnitude). Results are summarized in Supplementary Tables S4-S6. The magnitudes of smaller events ranges from 4.4 to 5.0 and their half-duration from 3 s to 7 s. Waveform fits presented in the Supplementary Figure S6-S10

show that joint moment tensor and force models usually perform better than single moment tensor or force sources.

5. Discussion and conclusion

In this study, we investigate the caldera collapse that affected the summit of Piton de la Fournaise in 2007. The sequence started on April 5 with a $M_w \sim 5.4$ VLP event visible at teleseismic distances. This event was then followed by 47 smaller collapses with similar source mechanisms. Using a moment tensor parameterization, the source of the first collapse is best represented by a vertically closing crack (cf., Fig. 3). Our results show that ring-faulting is not the dominant source mechanism as a CLVD source is unable to fit the observed VLP signals (Fig. S4; Shuler et al., 2013). Using a single force representation, the inversion yields an initially upwards vertical force that is consistent with the downward displacement of the rock column above the magma reservoir. This single force model fits the observations as well as a moment tensor source even if it relies on fewer model parameters (cf., Fig. 2a-b). Model selection using Akaike (AIC) and Bayesian (BIC) information criteria thus favor the simpler force model over a moment tensor description (see Supplementary Text S2 and Table S7). The joint inversion of force and moment tensor parameters suggests the combination of an initially upward vertical force and a closing crack. Despite its larger number of parameters, AIC and BIC criteria favor this joint model over previous source parameterization because it is more consistent with observations (especially at the near-field station RER, see Table S7). The combination of a moment tensor and a force also results in better waveform fits and lower AIC and

BIC values for smaller VLP events that followed the first collapse (see Supplementary Fig. S6-S10 and Table S8). Although the joint model seems to be the most appropriate according to AIC and BIC criteria, it is important to note that this solution is derived from noisy data and is affected by tradeoffs between source parameters. To evaluate the dependence of estimated quantities on the assumed parameterization, the different source representations will be taken into account in the following calculations.

A simple interpretation of the results presented above is that the collapsing crack source corresponds to the vertical contraction of the magma reservoir while the vertical force represents the resulting collapse of the overlying fractured rock column. This interpretation seems consistent with our joint source models showing that the closing crack source usually occurs before the vertical force is applied to the edifice (cf., Fig. 4 and Table S6). The combination of a collapsing crack and a single force has been already inferred to explain long-period signals observed on volcanoes (e.g., Nakano et al., 2003). Moreover, previous seismological and geodetic studies have shown that closing crack sources can correspond to magma chamber deflations during a caldera collapse (e.g., Riel et al., 2015; Mildon et al., 2016). The use of a single force has also been suggested to represent a subsiding caldera block (Kumagai et al., 2001).

Assuming a simple piston cylinder to represent the subsiding caldera block as illustrated in Fig. 6a, we can use the different source models discussed above to estimate the downward displacement of the collapsing rock column (cf., Supplementary Text S3). We assume a piston diameter of 500 m to ensure consistency with Urai et al. (2007) and Michon et al. (2011). The

piston extends vertically from the roof of the magma reservoir (at an elevation of ~ 300 m; Peltier et al., 2008; Duputel et al., 2019) to ~ 1700 m above sea level at the upper limit of CLVD and normal faulting events observed during the collapse sequence (Massin et al., 2011). For each model, we compute a lower-bound estimate of downward displacement for a density $\rho = 2.7 \text{ kg.m}^{-3}$ (taken from the velocity model used at OVPF) and an upper-bound using $\rho = 1.6 \text{ kg.m}^{-3}$ (according to the gravity study of Gailler et al., 2009). Moment tensor crack estimates use Lamé parameters $\lambda = 6 - 11 \text{ GPa}$ and $\mu = 8 - 13 \text{ GPa}$ corresponding to the aforementioned values of ρ along with P and S wave speeds derived from local velocity models (Battaglia et al., 2005; Mordret et al., 2015). The results shown in Fig. 6b and Fig. S11 indicate a total piston displacement ranging from $z \sim 180 \text{ m}$ to $z \sim 520 \text{ m}$ depending on the source model and the value of ρ . Interestingly, our joint source model produces consistent piston displacement estimates whether they are derived from moment tensor or force parameters. In this case, we estimate a total displacement $z \sim 340 \text{ m}$ assuming $\rho = 1.6 \text{ kg.m}^{-3}$, in agreement with direct observations reporting a depression depth of $\sim 330 \text{ m}$ in the Dolomieu crater (Michon et al., 2007; Urai et al., 2007). The single force model is associated with larger estimates (i.e., $z \sim 310 - 520 \text{ m}$) that are also consistent with field observations if we assume a denser piston cylinder. The moment tensor model under-estimates the observed collapse with $z \sim 180 - 300 \text{ m}$, even if larger predictions can be obtained assuming $\rho < 1.6 \text{ kg.m}^{-3}$ or a smaller piston. For simplicity, we will now assume $\rho = 1.6 \text{ kg.m}^{-3}$ for the moment tensor and joint model and $\rho = 2.7 \text{ kg.m}^{-3}$ for the single force model.

The above estimates of vertical displacement can be used to evaluate the

volume change of the magma reservoir after each collapse. Dividing this volumetric change by the time-delay T since the previous collapse, we obtain a volumetric change rate $\alpha = \Delta z S/T$ (where Δz is the downward displacement increment and S is the cross-sectional area at the base of the piston). This volumetric change rate shown in Fig. 6b can be compared directly to the magma outflow rate. It has been showed that the high-frequency ground motion velocity amplitude near the eruption site has similar evolution to the emission rate during the April 2007 eruption (Staudacher et al., 2009; Coppola et al., 2009; Michon et al., 2011). Using the approach of Hibert et al. (2015), we therefore estimate the magma outflow rate from continuous records at station TKR, located close to eruptive fissure (see Supplementary Text S4). The estimated lava extrusion rate shown in black in Fig. 6b is consistent with volumetric change rates estimated from our VLP catalog. This confirms that the 2007 Piton de la Fournaise collapse is primarily controlled by lateral magma withdrawal from the shallow reservoir.

As reported for other caldera collapses (e.g., Shuler et al., 2013), the duration of individual collapse events are significantly longer than what is typically observed for earthquakes of similar sizes. Our duration estimates ranges from 6 s to 14 s, while standard scaling laws (e.g., Duputel et al., 2013) predict durations ranging from 0.6 to 2 s for $M_w=4$ and $M_w=5$ earthquakes, respectively (cf., Supplementary Tables S4-S6). In addition, the source duration of VLP events does not seem to scale with their size. This clearly suggests that the underlying physical mechanism is not the same as earthquakes that are commonly observed on tectonic fault systems. Using a simple piston spring-block model (Kumagai et al., 2001), the duration of collapse

events is controlled by the geometry of the subsiding caldera block but also by the properties of the magma reservoir. In this model, the weight of the collapsing piston is balanced by friction on the surrounding ring fault and by pressure in the magma reservoir. When the magma reservoir depressurization exceeds static friction, the piston moves down into the chamber which suddenly increases its internal pressure and generate VLP signals. Assuming that the inter-event time-delay T is large compared to the duration of individual collapses, we can write (see Supplementary Text S5):

$$t_h = \frac{\pi}{2} \sqrt{\frac{\rho V_0 h}{\kappa S}} \quad (1)$$

where t_h is the piston source half-duration, V_0 is the initial volume of the magma reservoir and κ is the bulk modulus of the magma. Using geodetic estimates of the magma chamber volume (Peltier et al., 2008), we can interpret our estimates of t_h for each collapse to evaluate κ . Despite the large uncertainties, results shown in Fig. S12 typically ranges from $\kappa = 10^8$ Pa to $\kappa = 10^9$ Pa, which indicates that the magma in the reservoir was in a bubbly state during the caldera collapse (Huppert and Woods, 2002). The increase of source durations observed from April 6 to April 7 in Tables S4-S6 suggests a reduction of the magma bulk modulus implying that the magma becomes more bubbly. This might correspond to the exsolution of gas following the depressurisation of the chamber when a significant increase in the magma outflow rate is estimated (cf., Fig. 6b). Such interpretation seems consistent with field observations indicating a dramatic increase in the height of lava fountains to more than 200 m simultaneous with the reduction of κ and the increase of magma extrusion rate (Staudacher et al., 2009).

An interesting aspect of the 2007 Piton de la Fournaise collapse is the

evolution of the time-interval T between successive collapse increments shown in Fig. 6c. As reported previously (e.g., Michon et al., 2007), T gradually decreases from about 2 hours at the beginning of the collapse to ~ 30 min on April 6 at 12:00 GMT and then increases again until the end of the collapse. As detailed in text S5, the time-interval in our piston spring-block model can be expressed as:

$$T = \frac{2\Delta\mu F_n V_0}{\alpha\kappa S} \quad (2)$$

where $\Delta\mu$ is the difference between static (μ_S) and dynamic (μ_D) friction coefficients and F_n is the effective normal force exerted on the ring-fault delimiting the piston cylinder. Although the decrease of κ due to the exsolution of gas will tend to increase the time-interval between collapse events, the estimated variations of κ seems to have a moderate effect on T (as also inferred by Michon et al., 2011). On the other hand, we see in Fig. S13 that the variations of T can be partly explained by the increase of the magma outflow rate α . As noted by Stix and Kobayashi (2008) and Michon et al. (2011), the variations of time-interval are also controlled by changes in frictional resistance (i.e., $\Delta\mu F_n$ in eq. (2)). Fig. 6d shows the evolution of $\Delta F = \Delta\mu F_n$ estimated from collapse event durations and vertical displacements (see eq. (19) of the Supplementary Text S5). Fig. S14 shows that similar estimates of $\Delta\mu F_n$ can be obtained if we use the time-interval T and magma outflow α from seismic amplitudes (see eq. (20) of the Supplementary Text S5). These results suggest that the evolution of T can be explained by a decrease of the friction parameter $\Delta\mu F_n$ at the beginning of the collapse. As proposed by Michon et al. (2011), such an initial decrease of frictional resistance might correspond to the decrease of the effective normal force F_n caused by upward migrations

of hydrothermal fluids. Such weakening could also be caused by frictional melting or the activation of magma pockets intruding in the ring-fault system. Recent observations of exhumed caldera faults suggest that frictional melting play a critical role in caldera collapses (e.g., Han et al., 2019). Moreover, seismicity and field observations at Piton de la Fournaise show that the ring-fault system is a preferential path of magma intrusions (e.g., Staudacher, 2010; Duputel et al., 2019). Both interpretations seems plausible given satellite observations showing a ring-shaped thermal anomaly in the Dolomieu crater during summit subsidence and the existence of small lava flows emitted from the edge of the collapsed piston on April 6 (Urai et al., 2007).

The 2007 Piton de la Fournaise summit subsidence outlines the hazard caused by caldera collapses on basaltic volcanoes. In this context, a parameter of primary importance is the critical volume fraction of evacuated magma to trigger the collapse. According to the volume change derived after the first collapse, this critical volume fraction is only a few percent (between 1% and 4% of the shallow magma reservoir volume). This corresponds to critical underpressures in the magma chamber ranging from -7 to -40 MPa, which is in rough agreement with geodetic estimates (ranging from -5 to -10 MPa; Peltier et al., 2009; Got et al., 2013). It is interesting to notice that the 2007 Piton de la Fournaise collapse has characteristics that are similar to other basaltic caldera forming eruptions. The 1968 Fernandina, 2000 Miyakejima and 2018 Kilauea collapses are characterized by quasi-periodic series of incremental subsidence events manifested by tilt steps and VLP signals similar to what is observed at Piton de la Fournaise. These events are also driven by magma

withdrawal from shallow reservoirs through low-elevation eruptive vents. For both Fernandina and Kilauea, the time interval T between successive collapses follows an evolution that is quite similar to what is observed at Piton de la Fournaise (Stix and Kobayashi, 2008; Michon et al., 2011; Neal et al., 2019). Despite these similarities, there are also significant differences. For example, the total duration of the whole caldera collapse ranges from about 2 days at Piton de la Fournaise to more than 3 months at Kilauea. Some of these discrepancies can possibly be explained by differences in the summit caldera block geometry, reservoir volume, edifice strength, magma properties and lava extrusion rates. The relative importance of these different parameters are still poorly constrained given the challenging circumstances in which such collapses have been observed. New near-field seismogeodetic observations of the recent Kilauea summit subsidence therefore appear promising to better understand the mechanisms at the origin of caldera collapses.

Acknowledgments

This project was supported by the IPGS internal call for projects. This project has also received funding from the European Research Council (ERC, under the European Union’s Horizon 2020 research and innovation programme under grant agreement No 805256) and from Agence Nationale de la Recherche (project ANR-17-ERC3-0010). We thank Olivier Lengliné, Dimitri Zigone and Michael Heap for helpful discussions. Michel Tas is additionally thanked for grammatical assistance. This study incorporates data acquired by the Piton de la Fournaise Volcano Observatory (OVPF - IPGP) accessible via the VOLOBISIS Portal at <http://volobsis.ipgp.fr>. We also use seismic data

from GEOSCOPE (G), IRIS/IDA (II), IRIS/USGS (IU), Pacific21 (PS), Australian National Seismograph Network (AU), New China Digital Seismograph Network (IC) and Northeast Tibet Plateau experiment (Z1). We wish to thank the network and station operators for their commitment to collect high-quality seismic data.

References

- Bassin, C., Laske, G., Masters, G., 2000. The Current Limits of resolution for surface wave tomography in North America. *Eos Trans. AGU* 81.
- Battaglia, J., Ferrazzini, V., Staudacher, T., Aki, K., Cheminée, J.L., 2005. Pre-eruptive migration of earthquakes at the Piton de la Fournaise volcano (Réunion Island) 161, 549–558.
- Brenguier, F., Shapiro, N.M., Campillo, M., Ferrazzini, V., Duputel, Z., Coutant, O., Nercessian, A., 2008. Towards forecasting volcanic eruptions using seismic noise. *Nature Geosci.* 1, 126–130.
- Chouet, B.A., Dawson, P.B., James, M.R., Lane, S.J., 2010. Seismic source mechanism of degassing bursts at Kilauea Volcano, Hawaii: Results from waveform inversion in the 10–50 s band. *J. Geophys. Res.* 115, 716.
- Chouet, B.A., Matoza, R.S., 2013. A multi-decadal view of seismic methods for detecting precursors of magma movement and eruption. *J. Volc. Geoth. Res.* 252, 108–175.
- Coppola, D., Piscopo, D., Staudacher, T., Cigolini, C., 2009. Lava discharge

- rate and effusive pattern at Piton de la Fournaise from MODIS data. *J. Volc. Geoth. Res.* 184, 174–192.
- Duputel, Z., Ferrazzini, V., Brenguier, F., Shapiro, N., Campillo, M., Nercessian, A., 2009. Real time monitoring of relative velocity changes using ambient seismic noise at the Piton de la Fournaise volcano (La Reunion) from January 2006 to June 2007 *184*, 164–173.
- Duputel, Z., Lengliné, O., Ferrazzini, V., 2019. Constraining Spatiotemporal Characteristics of Magma Migration at Piton De La Fournaise Volcano From Pre-eruptive Seismicity. *Geophys. Res. Lett.* 46, 119–127.
- Duputel, Z., Tsai, V.C., Rivera, L., Kanamori, H., 2013. Using centroid time-delays to characterize source durations and identify earthquakes with unique characteristics. *Earth Planet. Sci. Lett.* 374, 92–100.
- Duputel, Z., Vergne, J., Rivera, L., Wittlinger, G., Farra, V., Hetényi, G., 2016. The 2015 Gorkha earthquake: A large event illuminating the Main Himalayan Thrust fault *43*, 2517–2525.
- Ekström, G., Stark, C.P., 2013. Simple Scaling of Catastrophic Landslide Dynamics *339*, 1416–1419.
- Epp, D., Decker, R.W., Okamura, A.T., 1983. Relation of summit deformation to East Rift Zone eruptions on Kilauea Volcano, Hawaii. *Geophys. Res. Lett.* 10, 493–496.
- Filson, J., Simkin, T., Leu, L.k., 1973. Seismicity of a caldera collapse: Galapagos Islands 1968. *Journal of Geophysical Research: Solid Earth (1978–2012)* 78, 8591–8622.

- Fontaine, F.R., Roult, G., Michon, L., Barruol, G., Di Muro, A., 2014. The 2007 eruptions and caldera collapse of the Piton de la Fournaise volcano (La Reunion Island) from tilt analysis at a single very broadband seismic station. *Geophys. Res. Lett.* 41, 2803–2811.
- Fontaine, F.R., Roult, G.C., Hejrani, B., Michon, L., Barruol, G., Tkalčić, H., Ferrazzini, V., Di Muro, A., Reymond, D., Peltier, A., Staudacher, T., Massin, F., 2016. Caldera Formation at the Piton de la Fournaise Volcano, La Réunion. AGU Fall Meeting, San Francisco .
- Ford, S.R., Dreger, D.S., Walter, W.R., 2010. Network Sensitivity Solutions for Regional Moment-Tensor Inversions. *Bull. Seism. Soc. Am.* 100, 1962–1970.
- Froger, J.L., Famin, V., Cayol, V., Augier, A., Michon, L., Lénat, J.F., 2015. Time-dependent displacements during and after the April 2007 eruption of Piton de la Fournaise, revealed by interferometric data. *J. Volc. Geoth. Res.* 296, 55–68.
- Gailler, L.S., Lénat, J.F., Lambert, M., Levieux, G., Villeneuve, N., Froger, J.L., 2009. Gravity structure of Piton de la Fournaise volcano and inferred mass transfer during the 2007 crisis. *J. Volc. Geoth. Res.* 184, 31–48.
- Got, J.L., Peltier, A., Staudacher, T., Kowalski, P., Boissier, P., 2013. Edifice strength and magma transfer modulation at Piton de la Fournaise volcano. *J. Geophys. Res.* 118, 5040–5057.
- Han, R., Kim, J.S., Kim, C.M., Hirose, T., Jeong, J.O., Jeong, G.Y., 2019.

- Dynamic weakening of ring faults and catastrophic caldera collapses. *Geology* 47, 107–110.
- Herrmann, R.B., 2013. Computer Programs in Seismology: An Evolving Tool for Instruction and Research. *Seismol. Res. Lett.* 84, 1081–1088.
- Hibert, C., Mangeney, A., Polacci, M., Muro, A.D., Vergnolle, S., Ferrazzini, V., Peltier, A., Taisne, B., Burton, M., Dewez, T., Grandjean, G., Dupont, A., Staudacher, T., Brenguier, F., Kowalski, P., Boissier, P., Catherine, P., Lauret, F., 2015. Toward continuous quantification of lava extrusion rate: Results from the multidisciplinary analysis of the 2 January 2010 eruption of Piton de la Fournaise volcano, La Réunion. *J. Geophys. Res.: Solid Earth* 120, 3026–3047.
- Huppert, H.E., Woods, A.W., 2002. The role of volatiles in magma chamber dynamics. *Nature* 420, 493–495.
- Kanamori, H., Given, J.W., 1981. Use of long-period surface waves for rapid determination of earthquake-source parameters. *Phys. Earth Planet. Inter.* 27, 8–31.
- Kanamori, H., Given, J.W., 1982. Analysis of long-period seismic waves excited by the May 18, 1980, eruption of Mount St. Helens- A terrestrial monopole 87, 5422–5432.
- Kanamori, H., Given, J.W., Lay, T., 1984. Analysis of seismic body waves excited by the Mount St. Helens eruption of May 18, 1980. *Journal of Geophysical Research: Solid Earth (1978–2012)* 89, 1856–1866.

- Kawakatsu, H., 1989. Centroid single force inversion of seismic waves generated by landslides. *Journal of Geophysical Research: Solid Earth* (1978–2012) 94, 12363–12374.
- Komatitsch, D., Tromp, J., 1999. Introduction to the spectral element method for three-dimensional seismic wave propagation. *Geophys. J. Int.* 139, 806–822.
- Kumagai, H., Ohminato, T., Nakano, M., Ooi, M., Kubo, A., Inoue, H., Oikawa, J., 2001. Very-Long-Period Seismic Signals and Caldera Formation at Miyake Island, Japan. *Science* 293, 687–690.
- Massin, F., Ferrazzini, V., Bachelery, P., Nercessian, A., Duputel, Z., Staudacher, T., 2011. Structures and evolution of the plumbing system of Piton de la Fournaise volcano inferred from clustering of 2007 eruptive cycle seismicity. *J. Volc. Geoth. Res.* 202, 96–106.
- Michon, L., Di Muro, A., Villeneuve, N., Saint-Marc, C., Fadda, P., Manta, F., 2013. Explosive activity of the summit cone of Piton de la Fournaise volcano (La Réunion island): A historical and geological review. *J. Volc. Geoth. Res.* 264, 117–133.
- Michon, L., Massin, F., Famin, V., Ferrazzini, V., Roult, G., 2011. Basaltic calderas: Collapse dynamics, edifice deformation, and variations of magma withdrawal. *Journal of Geophysical Research: Solid Earth* (1978–2012) 116, 8485.
- Michon, L., Staudacher, T., Ferrazzini, V., Bachelery, P., Marti, J., 2007.

- April 2007 collapse of Piton de la Fournaise: A new example of caldera formation. *Geophys. Res. Lett.* 34.
- Mildon, Z.K., Pugh, D.J., Tarasewicz, J., White, R.S., Brandsdóttir, B., 2016. Closing crack earthquakes within the Krafla caldera, North Iceland. *Geophys. J. Int.* 207, 1137–1141.
- Mordret, A., Rivet, D., Landès, M., Shapiro, N.M., 2015. Three-dimensional shear velocity anisotropic model of Piton de la Fournaise Volcano (La Réunion Island) from ambient seismic noise. *J. Geophys. Res.: Solid Earth* 120, 406–427.
- Nakano, M., Kumagai, H., Chouet, B.A., 2003. Source mechanism of long-period events at Kusatsu–Shirane Volcano, Japan, inferred from waveform inversion of the effective excitation functions. *J. Volc. Geoth. Res.* 122, 149–164.
- Neal, C.A., Brantley, S.R., Antolik, L., Babb, J.L., Burgess, M., Calles, K., Cappos, M., Chang, J.C., Conway, S., Desmither, L., Dotray, P., Elias, T., Fukunaga, P., Fuke, S., Johanson, I.A., Kamibayashi, K., kauahikaua, J., Lee, R.L., Pekalib, S., Miklius, A., Million, W., Moniz, C.J., Nadeau, P.A., Okubo, P., Parcheta, C., Patrick, M.R., Shiro, B., Swanson, D.A., Tollett, W., Trusdell, F., Younger, E.F., Zoeller, M.H., Montgomery-Brown, E.K., Anderson, K.R., Poland, M.P., Ball, J.L., Bard, J., Coombs, M., Dieterich, H.R., Kern, C., Thelen, W.A., Cervelli, P.F., Orr, T., Houghton, B.F., Ganseddi, C., Hazlett, R., Lundgren, P., Diefenbach, A.K., Lerner, A.H., Waite, G., Kelly, P., Clors, L., Werner, C., Mulliken, K., Fisher, G.,

- Damby, D., 2019. The 2018 rift eruption and summit collapse of Kilauea Volcano. *Science* 363, 367–+.
- Peltier, A., Famin, V., Bachelery, P., Cayol, V., Fukushima, Y., Staudacher, T., 2008. Cyclic magma storages and transfers at Piton de La Fournaise volcano (La Reunion hotspot) inferred from deformation and geochemical data. *Earth Planet. Sci. Lett.* 270, 180–188.
- Peltier, A., Staudacher, T., Bachelery, P., Cayol, V., 2009. Formation of the April 2007 caldera collapse at Piton de La Fournaise volcano: Insights from GPS data. *J. Volc. Geoth. Res.* 184, 152–163.
- Riel, B., Milillo, P., Simons, M., Lundgren, P., Kanamori, H., Samsonov, S., 2015. The collapse of Bardarbunga caldera, Iceland. *Geophys. J. Int.* 202, 446–453.
- Ritsema, J., Deuss, A., van Heijst, H.J., Woodhouse, J.H., 2011. S40RTS: a degree-40 shear-velocity model for the mantle from new Rayleigh wave dispersion, teleseismic traveltime and normal-mode splitting function measurements. *Geophys. J. Int.* 184, 1223–1236.
- Shuler, A., Ekström, G., Nettles, M., 2013. Physical mechanisms for vertical-CLVD earthquakes at active volcanoes. *J. Geophys. Res.: Solid Earth* 118, 1569–1586.
- Sigmundsson, F., Hooper, A., Hreinsdóttir, S., Vogfjord, K.S., Ofeigsson, B.G., Heimisson, E.R., Dumont, S., Parks, M., Spaans, K., Gudmundsson, G.B., Drouin, V., Arnadóttir, T., Jonsdóttir, K., Gudmundsson, M.T.,

- Hognadóttir, T., Fridriksdóttir, H.M., Hensch, M., Einarsson, P., Magnússon, E., Samsonov, S., Brandsdóttir, B., White, R.S., Agustsdóttir, T., Greenfield, T., Green, R.G., Hjartardóttir, A.R., Pedersen, R., Bennett, R.A., Geirsson, H., La Femina, P.C., Björnsson, H., Pálsson, F., Sturkell, E., Bean, C.J., Mollhoff, M., Braiden, A.K., Eibl, E.P.S., 2015. Segmented lateral dyke growth in a rifting event at Bardarbunga volcanic system, Iceland. *Nature* 517, 191–U158.
- Staudacher, T., 2010. Field observations of the 2008 summit eruption at Piton de la Fournaise (Ile de La Réunion) and implications for the 2007 Dolomieu collapse. *J. Volc. Geoth. Res.* 191, 60–68.
- Staudacher, T., Ferrazzini, V., Peltier, A., Kowalski, P., Boissier, P., Catherine, P., Lauret, F., Massin, F., 2009. The April 2007 eruption and the Dolomieu crater collapse, two major events at Piton de la Fournaise (La Reunion Island, Indian Ocean). *J. Volc. Geoth. Res.* 184, 126–137.
- Stix, J., Kobayashi, T., 2008. Magma dynamics and collapse mechanisms during four historic caldera-forming events. *Journal of Geophysical Research: Solid Earth* (1978–2012) 113.
- Takei, Y., Kumazawa, M., 1994. Why have the single force and torque been excluded from seismic source models? *Geophys. J. Int.* 118, 20–30.
- Uhira, K., Yamasato, H., Takeo, M., 1994. Source mechanism of seismic waves excited by pyroclastic flows observed at Unzen volcano, Japan. *J. Geophys. Res.* 99, 17757–17773.

Urai, M., Geshi, N., Staudacher, T., 2007. Size and volume evaluation of the caldera collapse on Piton de la Fournaise volcano during the April 2007 eruption using ASTER stereo imagery. *Geophys. Res. Lett.* 34.

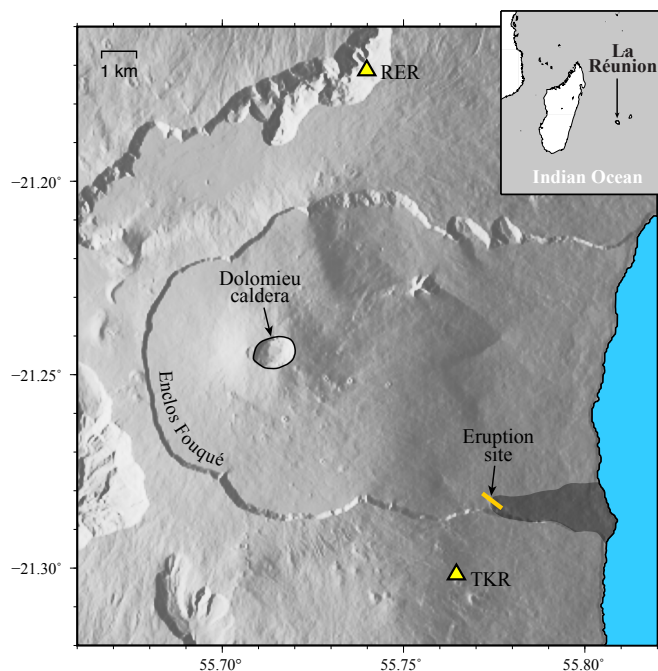


Figure 1: **Location of the Piton de la Fournaise volcano.** The April 2007 collapse occurred in the Dolomieu crater located at the summit of the Piton de la Fournaise central cone. The eruptive fissure of April 2007 is indicated with an orange line and the corresponding lava flow is outlined in dark grey. Yellow triangles indicate the location of stations RER and TKR used in the present study.

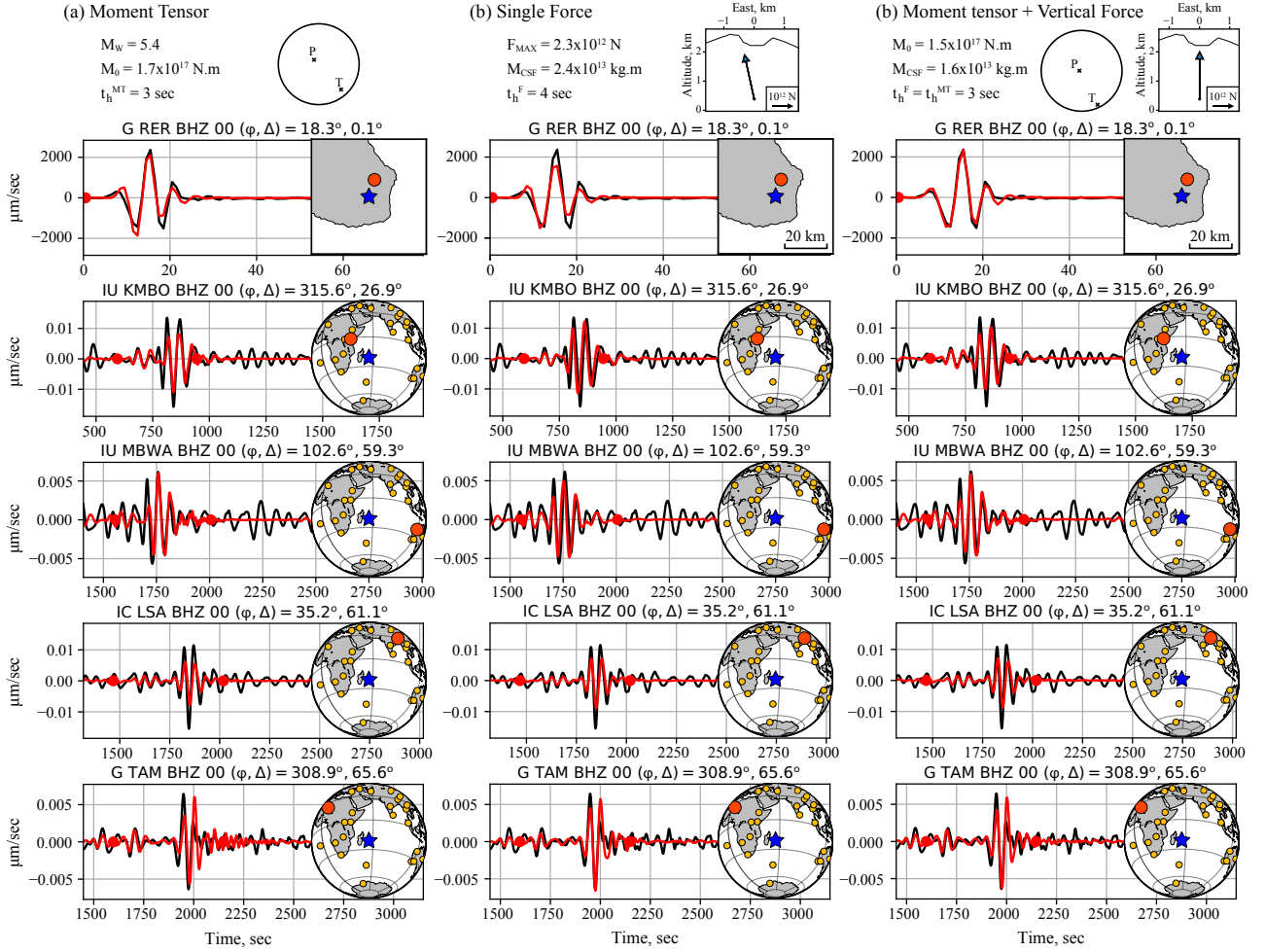


Figure 2: **Different source representations tested for the first caldera collapse on April 5, 2007.** Source models are presented on top for (a) the moment tensor inversion, (b) the single force inversion and (c) the joint moment tensor and force solution. t_h^{MT} and t_h^F are respectively the moment-tensor and force half-durations. M_w is the moment magnitude, M_0 is the scalar seismic moment, F_{MAX} is the maximum force and M_{CSF} is the CSF value (cf., Kawakatsu, 1989). Comparison between data (black) and synthetic (red) traces are shown for representative stations. The part of the waveform used for source inversion is delimited by red dots. Yellow circles in right insets show the distribution of stations used for the inversion while the red circle indicate the location of the station whose waveform is presented. The station azimuth (ϕ) and epicentral distance (Δ) is indicated on top of each seismic trace.

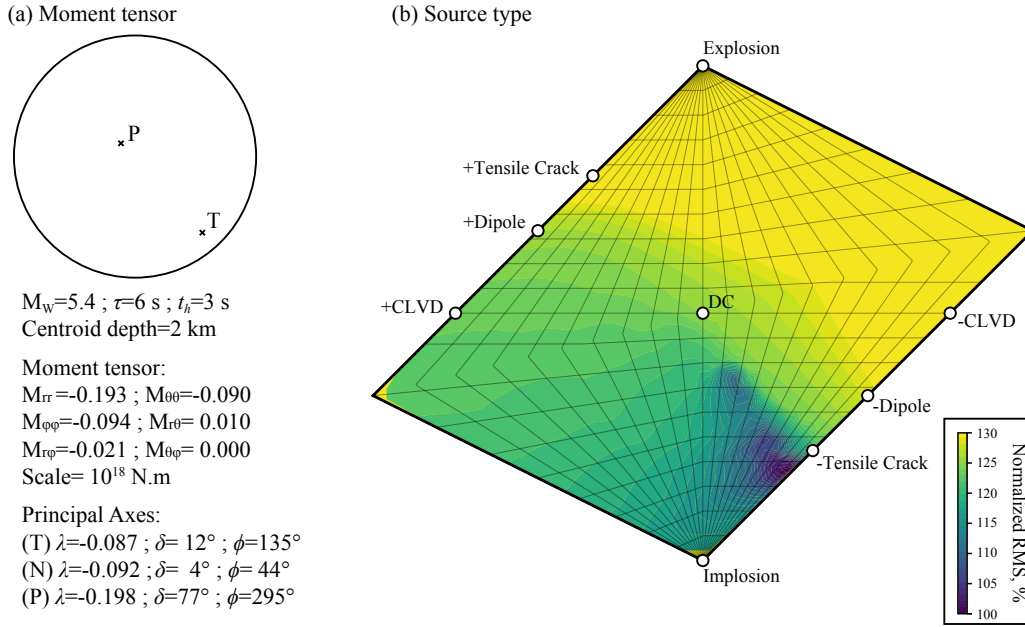


Figure 3: **Moment tensor solution for the first Piton de la Fournaise caldera collapse on April 5, 2007.** (a) Preferred moment tensor solution. The half-duration $t_h=3$ s and the centroid time-shift is $\tau=6$ s with respect to 20:48:43UTC. λ , δ and ϕ indicate respectively the eigenvalue, plunge and azimuth angles of the principal axes. Moment tensor components and eigenvalues are scaled by a factor of 10^{18} N.m. (b) Source type plot showing the Normalized RMS misfit corresponding to different types of moment tensor sources (see Supplementary Text S1). The optimum solution presented in (a) is indicated by a white star. The corresponding waveform fits are presented in Fig. 2a and S15.

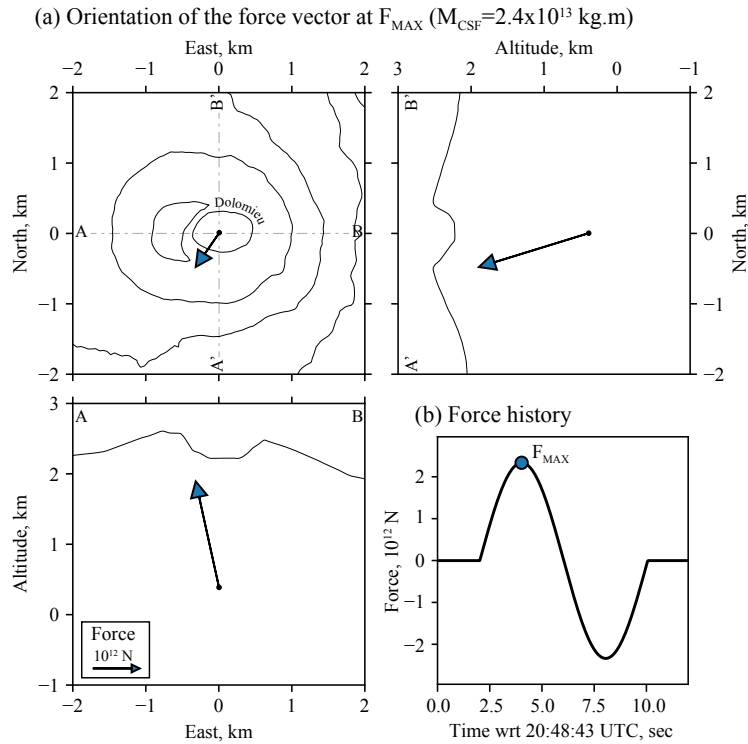


Figure 4: **Single force solution for the first Piton de la Fournaise caldera collapse on April 5, 2007.** (a) Initial orientation of the peak force vector (i.e., at F_{MAX}). Force scale is indicated on the lower left panel. (b) Force time-history. The blue dot labeled F_{MAX} indicate the time when the force is maximum (i.e., the initial peak force). Waveform fit are presented in Fig. 2b and S16.

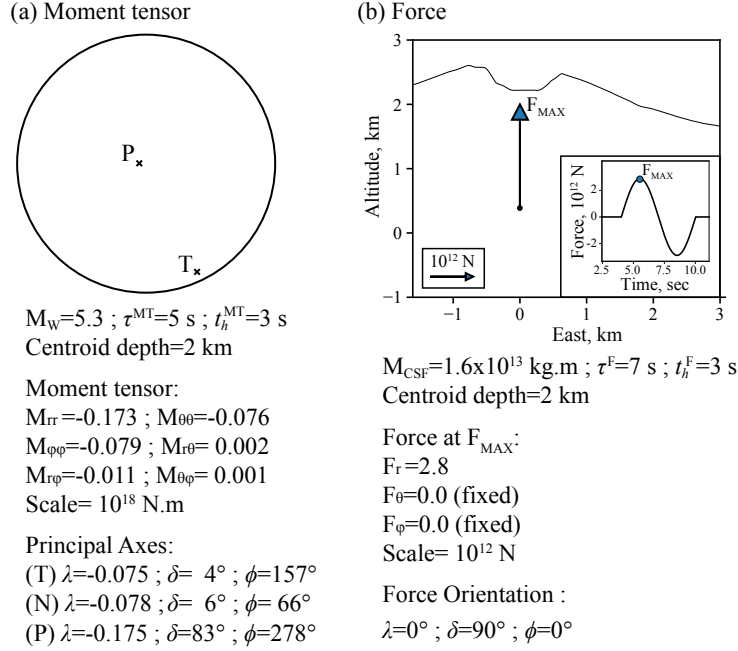


Figure 5: **Joint Moment Tensor and Force solution for the first Piton de la Fournaise caldera collapse on April 5.** (a) Moment tensor parameters. (b) Force parameters. t_h^{MT} and t_h^F denote the half-duration of the moment tensor and force source, respectively. The centroid time-shift of the moment tensor (τ^{MT}) and force (τ^F) are defined with respect to 20:48:43UTC. λ , δ and ϕ indicate respectively the eigenvalue or force, plunge and azimuth angles of the principal axes. The lower right inset in (b) indicate the force time history. The blue dot labeled F_{MAX} indicate the time when the force is maximum (i.e., the initial peak force). Waveform fit are presented in Fig. 2c and S17.

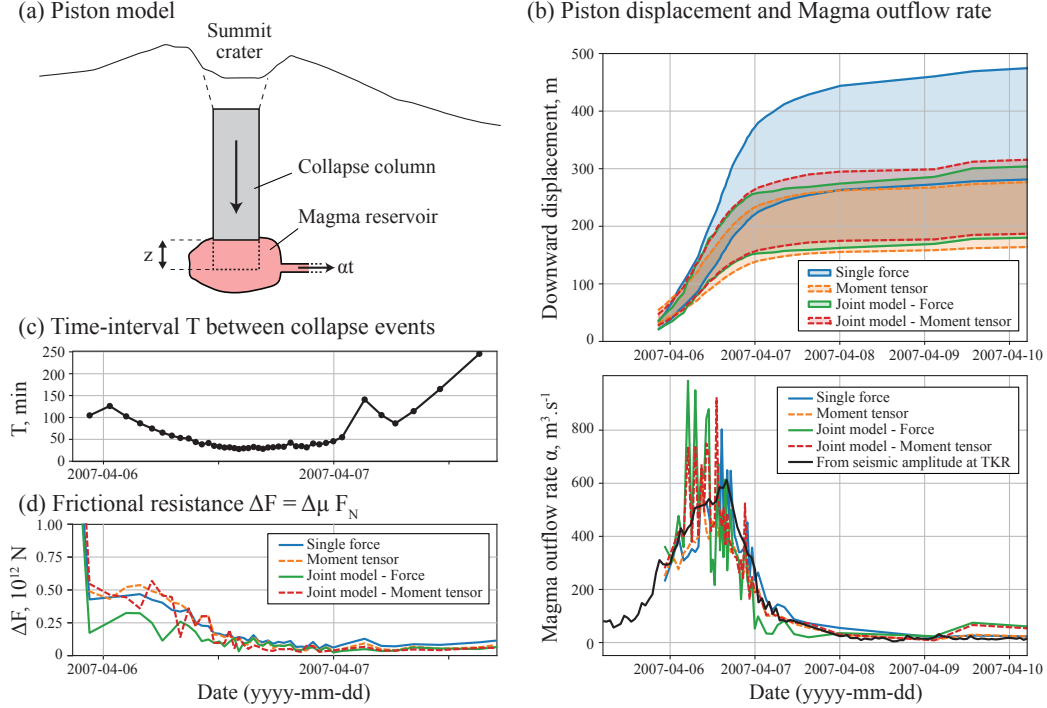


Figure 6: **Piston source model.** (a) A schematic diagram of the source model used to explain very-long-period signals observed at Piton de la Fournaise. (b) Piston downward displacement (z) and magma outflow rate (α). The full time evolution of the cumulative displacement between April 5 and April 14 is shown in the Supplementary Fig. S11. (c) Time-interval between successive collapse events in our catalog. (d) Frictional resistance $\Delta F = \Delta\mu F_N$, corresponding to the difference between static and dynamic friction (see Supplementary Text S5). The different colors in (b) and (d) correspond to the different source models obtained in sections 3 and 4. The upper and lower bound estimates of Δz in (b) correspond respectively to $\rho = 1.6 \text{ kg} \cdot \text{m}^{-3}$ and $\rho = 2.7 \text{ kg} \cdot \text{m}^{-3}$. The estimates of α and ΔF are based on $\rho = 2.7 \text{ kg} \cdot \text{m}^{-3}$ for the single force model and $\rho = 1.6 \text{ kg} \cdot \text{m}^{-3}$ for the other models (see main text). The black line shown in the bottom subfigure of (b) corresponds to the magma extrusion rate estimated from seismic amplitudes observed at station TKR (see main text and Supplementary Text S3)